MCC950 regulates stem cells destiny through modulating SIRT3-NLRP3 inflammasome dynamics during oxygen glucose deprivation

Ravi Prakash[1], Neha Kumari[1], Abu Junaid Siddiqui[1], Abdul Quaiyoom Khan[2], Mohsin Ali Khan[3], Rehan Khan[4], Rizwanul Haque[5], Avril AB Robertson[6], Johannes Boltze[7], Syed Shadab Raza[*1,8]

[1]Laboratory for Stem Cell & Restorative Neurology, Department of Biotechnology, Era's Lucknow Medical College and Hospital, Era University, Sarfarazganj, Lucknow−226003, India

[2]Translational Research Institute, Academic Health System, Hamad Medical Corporation, P.O. Box 3050, Doha, Qatar

[3]Era University, Sarfarazganj, Lucknow−226003, India

[4]Chemical Biology Unit, Institute of Nano Science and Technology, Mohali, Punjab 140306, India

[5]Departmenyt of Biotechnology, Central University of South Bihar, Gaya -824236, India

[6]School of Chemistry and Molecular Biosciences, The University of Queensland, Brisbane, QLD, Australia

[7]School of Life Sciences, University of Warwick, Coventry, UK

[8]Department of Stem Cell Biology and Regenerative Medicine, Era's Lucknow Medical College Hospital, Era University, Sarfarazganj, Lucknow−226003, India

Running Title: MCC950 regulates stem cells destiny in experimental ischemic stroke

Correspondence:

Dr. Syed Shadab Raza

drshadab@erauniversity.in

Lab: +91–0522–6600777 Extn. 119

Fax: +91–0522–2407824

Abstract

Ischemic stroke is the major cause of death and morbidity worldwide. Stem cell treatment is at the forefront of ischemic therapeutic interventions. However, the fate of these cells following transplantation is mostly unknown. The current study examines the influence of oxidative and inflammatory pathological events associated with experimental ischemic stroke (oxygen glucose deprivation (OGD)) on the stem cell population (human Dental Pulp Stem Cells, and human Mesenchymal Stem Cells) through the involvement of the NLRP3 inflammasome. We explored the destiny of the above-mentioned stem cells in the stressed micro (-environment) and the ability of MCC950 to reverse the magnitudes. An enhanced expression of NLRP3, ASC, cleaved caspase1, active IL-1β and active IL-18 in OGD-treated DPSC and MSC was observed. The MCC950 significantly reduced NLRP3 inflammasome activation in the aforementioned cells. Further, in OGD groups, oxidative stress markers were shown to be alleviated in the stem cells under stress, which was effectively relieved by MCC950 supplementation. Interestingly, whereas OGD increased NLRP3 expression, it decreased SIRT3 levels, implying that these two processes are intertwined. In brief, we discovered that MCC950 inhibits NLRP3-mediated inflammation by inhibiting the NLRP3 inflammasome and increasing SIRT3. To conclude, according to our findings, inhibiting NLRP3 activation while enhancing SIRT3 levels with MCC950 reduces oxidative and inflammatory stress in stem cells under OGD-induced stress. These findings shed light on the causes of hDPSC and hMSC demise following transplantation and point to strategies to lessen therapeutic cell loss under ischemic-reperfusion stress.

Keywords: Ischemic Stroke, MCC950, Oxygen Glucose Deprivation, Stem cell survival and death, Dental Pulp Stem Cells, Mesenchymal Stem Cells

Introduction

Stroke is a prominent cause of death and disability in adults. These debilitating diseases have a massive disease burden, both in terms of health suffering and economic costs [1, 2]. Neurons and microglia/macrophages are well known to play important roles in the production of pro-inflammatory cytokines and the inflammatory cascades triggered by ischemic stroke [3-5]. In brief, within hours of an ischemic stroke, microglia, macrophages, and astrocytes are activated, leading to the production of cytokines and chemokines [6] and the influx of leukocytes [7, 8]. Inflammatory cytokines promote leukocyte entry into brain tissue, triggering an inflammatory cascade response in which activated microglia and infiltrating leukocytes produce more inflammatory mediators, such as the nucleotide-binding oligomerization domain-like receptor protein 3 (NLPR3) inflammasome, causing brain edema and hemorrhage, increasing blood-brain barrier damage and promoting more neuronal death [9]. In stroke, the most commonly studied inflammasome is the NLRP3 inflammasome [10]. Despite the fact that various anti-inflammatory agents have shown great promise in the treatment of ischemic injury, the majority of them have failed [11]. As a result, new therapies aimed at inhibiting inflammation and thus rescuing cells are urgently needed to improve therapeutic outcomes.

Stem cell therapy is a promising treatment option for ischemic stroke [12-14]. Clinical investigations with these cells, in contrast to experimental findings, have so far given poor results [15-17], presumably due to stem cell malfunction and limited vitality [18-20]. The fate of these cells in the ischemic milieu is largely unknown due to a lack of understanding of the mechanism by which the microenvironment regulates their destiny. It is critical to remember that transplanted cells follow the same rules as cells of the oxidative and inflammatory microenvironment. Along these lines, the current study sought to determine whether the local environment influences the fate of stem cells and whether MCC950, an NLRP3 inflammasome inhibitor, can reverse these processes. MCC950 is the most specific NLRP3 inhibitor available. It does not inhibit NLRP1, NLRC4, or AIM2 inflammasomes [21]. MCC950 binds to NLRP3, hence stopping it from hydrolyzing ATP and preventing it from keeping its active structural shape. This stops NLRP3 from causing ASC to oligomerize and decreases caspase-1 cleavage. MCC950 also prevents the release of IL-1β caused by NLRP3 activators such as nigericin, ATP, and MSU crystals [22, 21]. By specifically focusing on the NLRP3 NATCH domain and interfering with the Walker B motif, MCC950 prevents NLRP3 from changing its conformation

and oligomerizing thus blocking inflammasome function [23, 24]. Based on previous research indicating that ischemic stroke has a negative impact on brain cells [25, 26] as well as stem cells [27, 28], we propose that NLRP3 regulates the fate of stem cells during ischemic stress and that MCC950 has the potential to rescue these cells under such conditions.

Material and Methods

Chemicals and reagents

The drugs, activators, and inhibitors used in this investigation are listed in supplementary table 1, the chemicals used are described in supplementary table 2, and antibodies are given in supplementary table 3.

Cell line maintenance

Human Dental Pulp Stem Cell (cat # CL008; DPSC) and human mesenchymal stem cells (cat # CL001; MSC) were purchased from Himedia Laboratories Pvt. Ltd. The cells were cultured in a humidified CO_2 incubator (5% CO_2, 37°C) in Dulbecco's Modified Eagle's Medium with 10% fetal bovine serum, 100 U/mL penicillin, and 100 mg/mL streptomycin. The cells were routinely sub-cultured after reaching a confluence of 70%-80%.

Oxygen Glucose Deprivation treatment

To mimic an ischemic stroke *in vitro*, the DPSC and MSC were subjected to the oxygen glucose deprivation (OGD) treatment. In a 6 well plate, the cells were seeded at a density of 1×10^6 cells per well and incubated at 65%-70% confluence under standard culture conditions. The growth media was then replaced with OGD medium (a medium devoid of FBS, glucose, and sodium pyruvate) and incubated for 30 minutes in the incubator. The cells were then placed in a hypoxic chamber (Stem Cell Technologies, Cambridge, MA, USA, 27310) with 1% O_2, 5% CO_2, and 94% N_2 atmosphere. In a CO_2 incubator, the hypoxic chamber was incubated for 12 hours. Afterward, the OGD medium was replaced with normal culture medium, and the cells were grown for another 24 hours under normal conditions before the assays were done.

Measurement of intracellular $O_2^{\bullet-}$ generation

The Dihydroethidium (DHE) staining method was used to identify intracellular $O_2^{\bullet-}$ production. In brief, DPSC and MSC were seeded in 12 well plates with sterile cover slips at a density of $2x10^4$ DPSC or MSC/well and allowed to grow overnight under standard culture conditions. After reaching 65%-70% confluency, the DPSC and MSC were given their treatments, which included OGD followed by normoxia. Following the desired treatment, DPSC and MSC were washed with 1X PBS and stained in serum-free media for 30 minutes in the dark with DHE (10µM). After incubation, the DHE solution was replaced with fresh 1X PBS (pre-warmed), and the DPSCs and MSCs were examined under an inverted fluorescent microscope.

Measurement of intracellular H_2O_2 generation

According to the manufacturer's instructions, Amplex Red was used to calculate intracellular H_2O_2. In a nutshell, OGD was performed on DPSC and MSC in the presence and absence of MCC950. The DPSC and MSC were then scraped into RIPA buffer and incubated on ice for 30 minutes, followed by centrifugation at 20,000×g for 30 minutes at 4°C temperature. The supernatant was collected and the H_2O_2 concentration was calculated. Following that, 50 µl of supernatant were mixed with 50 µl of reaction mixture (Amplex Red 100 µM, HRP-0.2 U/mL in sodium phosphate buffer, pH 7.4) and incubated at room temperature for 30 minutes. At 560 nm, the absorbance was measured, and the H_2O_2 concentration was calculated by extrapolating the absorbance against the H_2O_2 standard curve (1-5 µM).

Analysis of total ROS production

DPSC and MSC were seeded in 12 well plates with sterile cover slips at a density of $2x10^4$ DPSC or MSC/well and allowed to grow overnight under standard culture conditions. After reaching 65%-70% confluency, the DPSC and MSC were given their treatments, which included OGD followed by normoxia. Following the desired treatment, DPSC and MSC were washed with 1X PBS and stained in serum-free media for 30 minutes in the dark with DCFDA (10 µM). After incubation, the DCFDA solution was replaced with fresh 1X PBS (pre-warmed), and the DPSCs and MSCs were examined under an inverted fluorescent microscope.

DPSC and MSC morphology analysis

A morphological study was performed to investigate the effect of hypoxia-glucose deprivation on the structure of DPSC and MSC. The DPSC and MSC were seeded at a density of 1×10^5 per well in 12 well plates on poly-L-lysine coated coverslips and incubated for 18–20 hours. The OGD treatment was given in the manner described in the section on OGD treatment protocol. The morphological changes were examined using an inverted microscope (Axio-Observer, ZEISS, Germany).

Cell viability assay by trypan blue dye exclusion test

The cell death of MSC after OGD treatment was determined using the trypan blue dye exclusion assay. The cells were seeded in 96 well plates at a density of $1x10^4$ cells per well and allowed to develop for 18–20 hours. Before being placed in normoxia, the cells were given an OGD treatment. Cells were extracted from each well using trypsinization (incubation with 0.25% Trypsin-EDTA for 3 minutes at 37 °C) and centrifugation at 300×g for 5 minutes. To minimise cell loss, the culture medium from the same group of wells was pooled and centrifuged prior to trypsinization to collect any floating cells, which were then mixed with trypsinized harvested cells. Finally, cells were stained with trypan blue dye and counted for dye-positive and dye-negative cells using a hemocytometer under an inverted microscope. The percentage of cell death for each cell category was compared to the total number of cells in each category.

MTT cell viability assay

The MTT assay was also used to test cell survival. The DPSC and MSC were seeded in 96 well plates at a density of $2x10^4$ cells per well and subjected to OGD and normoxia treatments as previously described. Furthermore, 5 µl of MTT solution (5 mg/ml in 1X PBS, pH 7.4) was added to each well and incubated for 3 hours under standard culture conditions. The formazan crystals formed within viable cells were dissolved in DMSO (100 µl), and the absorbance at 595 nm was measured using a microplate reader (iMark, BioRad, Gurugram, India). The findings were presented as a percentage of the treatment groups' surviving in comparison to the control group.

TUNEL staining

DPSC received the desired treatments, as indicated in the previous sections. Then fixed cells were TUNEL-labelled by using the Apo-BrdU TUNEL Assay kit (Invitrogen) following the manufacturer's directions.

Immunocytochemistry

Fluorescence immunocytochemistry was performed on DPSC and MSC cell cultures in 12 well plates. Following the appropriate procedures, the cultures were rinsed in 1X PBS before being fixed for 10 minutes at room temperature in 1% paraformaldehyde. After washing the cells thrice with 1X PBS, nonspecific binding was blocked by using 1% bovine serum albumin and 0.3% Triton-X-100 in 1X PBS for 1 hour. The cells were then incubated with primary antibodies diluted in blocking buffer overnight at 4°C. The cells were then incubated with secondary antibodies. The nuclei of the cells were counterstained with 4′6′-diamidino-2-phenylindole (DAPI, 0.5g/ml) (Sigma-Aldrich). Immunofluorescence was imaged using a fluorescence microscope (Zeiss Axio-Observer Z1).

qRT-PCR analysis

Total RNA was extracted from hDPSCs using the Trizol reagent in accordance with the manufacturer's instructions. In each experiment, an equal amount of RNA (approximately 1 μg) was reverse transcribed using SuperScript® III RT cDNA synthesis. Following that, 1 μl of appropriately diluted cDNA was used as a template for RT-PCR analyses with Taqman Gene Expression Assays. For NLRP3 and GAPDH, the PCR reaction was performed with 1X Taqman gene assays (provided 20X). The PCR steps were as follows: Incubation at 50°C for 10 minutes, followed by 40 cycles of denaturation at 94°C for 20 seconds and annealing and extension at 60°C for 60 seconds. The chemical dilutions are shown in Table ST4.

Western blotting

All of the experimental samples (DPSC and MSC) were lysed with RIPA lysis buffer to estimate the protein. The cells were given an appropriate volume of ice-cold lysis solution supplemented with protease and phosphatase inhibitors, mixed properly, and stored on ice for 30 minutes. After the isolation and estimation of the protein samples, the Western blots on these samples were performed as per the standard laboratory protocol. ImageJ software was used to assess the

intensity of bands, which was then corrected using GAPDH data and expressed as a fold change in protein expression.

Statistical analysis

In all experiments, "n" represents the number of independent experiments. At least four independent experiments (n=4) were conducted to collect data, except for the figure S4 (n=3). For imaging data sets, we used at least 50 cells per group per experiment. Data distribution was checked by the Shapiro-Wilk test of normality. One way analysis of variance (ANOVA) with the Newman-Keuls test (for normally distributed data); the Kruskal-Wallis test followed by Dunn's test for multiple comparisons (for non-normally distributed data) were used to test statistical differences with sufficient post hoc analysis using SPSS statistics 28.0 software (IBM). 0.05 was considered statistically significant (*/$^{\#}$P<0.05, **/$^{\#\#}$P<0.01, and ***/$^{\#\#\#}$P<0.001 compared to the control/ OGD/Activators/Inhibitors-treated group).

Results

MCC950 abrogates OGD induced oxidative stress in DPSC and MSC through suppressing NLRP3 inflammasome activation

Oxidative stress, involving increased ROS generation, is a central feature of ischemic stroke [29]. Along these lines, we investigated whether activation of the NLRP3 inflammasome by OGD causes the induction of oxidative stress. In brief, the effects of oxidative stress during OGD in cultured DPSC and MSC were investigated using DHE, Amplex Red, and DCFDA staining. Both DPSC (Figure 1A, B, and C) and MSC (Figure 1D, E, and F) produced abrupt amounts of $O_2^{\bullet-}$, H_2O_2, and total ROS as a whole, after 12 hours of OGD followed by 24 hours of normoxia. When DPSC and MSC were treated with MCC950 (a selective NLRP3 inhibitor), lower levels of $O_2^{\bullet-}$, H_2O_2 and total ROS were found compared to OGD alone treated cells. We used NLRP3 specific siRNAs to confirm that the MCC950 precisely targeted the NLRP3 inflammasome pathway and that inhibiting the NLRP3 cascade depletes oxidative stress as observed above. The use of NLRP3-siRNAs reduced intracellular $O_2^{\bullet-}$, H_2O_2, and total ROS generation in DPSC, thus confirming the participation of NLRP3 inflammation and the anti-oxidative effect of MCC950 (Figures S1A-C). Lipopolysaccharides (LPS), known to be an activator of the NLRP3 inflammasome [30, 31] and have also been linked to free radical production [32], was used to

test the hypothesis that NLRP3 inflammation is related to the oxidative stress observed in our case. Previous findings indicate that a dose of LPS (such as 1 µg/ml) supplies both the priming signal and the activation signal, leading to NLRP3 inflammasome and mature IL-1β secretion [33, 34]. Similar dose of LPS were used in this study.

Furthermore, we observed a significant effect of OGD treatment on the morphology of the DPSC and MSC. In summary, morphological analysis of OGD or LPS-treated DPSC and MSC revealed nuclei shrinkage, rounding, and fragmentation, as well as condensation. The morphology of the DPSC and MSC was observed to be identical to the control group cells after MCC950 treatment of the OGD challenged cells (Figures 1G and H). To verify the above findings, DPSCs were subjected to OGD in the presence and absence of NLRP3-siRNA (Supplementary Figure S1D). The results were in line with the morphology observed in OGD, LPS, and MCC950 treated cells.

MCC950 impedes the OGD promoted NLRP3 inflammasome activation in DPSC and MSC

To see if OGD therapy activated the NLRP3 inflammasome in DPSC, we looked at the expression of the NLRP3 inflammasome protein complex. In brief, we quantified the expression of NLRP3, ASC, cleaved caspase1, IL-1β, and IL-18 through western blotting. LPS served as positive control for the NLRP3 inflammasome cascade. DPSCs were exposed to MCC950 after OGD treatment, to confirm the potential involvement of the NLRP3 inflammasome in OGD-induced inflammatory stress in DPSCs and to check the reparative effect of the MCC950 against the OGD induced inflammation. As indicated in Figure 2A, OGD induced NLRP3, ASC, and cleaved casapase-1 activation, and IL-1β, and IL-18 secretions were significantly abolished by MCC950 in DPSC as well as in MSC. Transfection with NLRP3-siRNA also inhibited OGD induced expression of NLRP3, ASC, and cleaved caspase1 expression (Figure S2A and B).

To confirm that NLRP3 inflammasome activation is a common event in stem cells in response to acute oxidative stress, we examined the NLRP3 inflammasome response in MSC after OGD treatment. Similar findings were observed in the case of MSC when they were given OGD treatment. In brief, as represented in Figure 2B, OGD promoted the expression of NLRP3 inflammasome linked proteins. Though MCC950 supplementation resulted in a significant decrease in the expression of these proteins, indicating NLRP3 inflammasome reversal. The

collective results suggested that MCC950 depleted the cellular NLRP3 inflammasome activation in MSC.

To reconfirm the results obtained with the DPSC and MSC with the supplementation of the MCC950, we measured NLRP3 and cleaved caspase1 protein levels via fluorescent imaging in DPSC (Figure 2C and D) and MSC (Figure 2E and F). The expression of NLRP3 and the cleaved caspase1 were both increased in the OGD group. Notably, IL-1β and IL-18, which are cleaved to active form by cleaved caspase1, were also increased after OGD but limited by MCC950 treatment (Figure 2A and B). These findings confirm that MCC950 treatment is capable of effectively inhibiting NLRP3 inflammasome activation in stem cells *in vitro*.

MCC950 reverse the death ratio in DPSC and MSC

Ischemic stroke pyroptosis is known to be caused by the NLRP3-caspase1 pathway [35, 36]. We investigated the link between OGD-induced inflammatory stress, NLRP3 inflammasome, cell viability, and MCC950 along these lines. In brief, we evaluated the MTT assay, Tunel staining, and Trypan blue exclusion live-death cell assay, and we observed that MCC950 was able to prevent pyroptosis in both DPSC and MSC (Figure 3A-D). In summary, a 12 hour hypoxia-glucose deprivation followed by a 24 hour period of normoxia increased the expression of DPSC cellular death number as measured by MTT (an enzymatic measure of active mitochondrial respiration), as observed by the formazan coloured solution, which has a lower intensity than the control. In comparison to the OGD alone treated DPSC, the addition of MCC950 resulted in a large proportion of metabolically active cells (Figure 3A). Likewise, when the DPSCs were tested for the Tunel assay (a method to detect DNA fragments), similar results were reported. Tunel's samples were examined using an inverted fluorescence microscope. In summary, the OGD-DPSCs had a higher number of DNA fragmented cells than the control DPSCs, but the MCC950 supplementation significantly reduced the DNA break in the MCC950 treated OGD-DPSCs compared to the OGD-alone treated DPSCs, as evidenced by lower anti-BrdU positive signals (Figure 3B). The LPS-treated DPSCs had the same result as the OGD-treated DPSCs.

MSCs were used to confirm the above findings. The MTT results from the MSCs setting backed the findings from the DPSCs viability experiments. In brief, the MCC950 treated OGD

challenged MSC showed higher cell viability compared to the OGD alone treated cells (Figure 3C). Furthermore, the application of Trypan blue exclusion dye demonstrated that the 12 hours of OGD followed by 24 hours of normoxia resulted in a large number of cell deaths, which were subsidised by the addition of MCC950 (Figure 3D). In summary, when compared to the control or the OGD+MCC950 treated MSCs, the OGD treated MSCs exhibit a high trypan blue positive number. Again, the LPS were used as a positive control.

MCC950 reduces the activation of mitochondrial ROS in DPSC and MSC

Mitochondrial ROS has been linked to NLRP3 inflammasome activation and has been implicated in OGD-treated stress [37, 38]. As a result, we decided to focus on the potential role of mitochondrial ROS, as well as the effect of MCC950 supplementation on mitochondrial ROS activation in OGD-induced DPSC and MSC. The mito-SOX and mito-Green staining revealed an abrupt generation of ROS in the mitochondria of OGD-treated DPSC and MSC both. While MCC950 treatment to both cell types after OGD treatment significantly subsidized the mito-SOX signalling, and this was an indication of lower ROS generation. MCC950's inhibitory effect on mtROS generation was confirmed by the employment of mito-Tempo in parallel to the MCC950 treated cells. The use of mito-Tempo also revealed that mtROS is a trigger of NLRP3 inflammasome activation in both DPSC and MSC (Figures 4A and B).

MCC950 inhibits OGD-induced NLRP3 activation by activating SIRT3 in human DPSC and MSC

Next, we examine the SIRT3 expression in DPSC and MSC in context with the expression of NLRP3. SIRT3, a mitochondrial sirtuin that deacetylates substrates implicated in both ROS generation and detoxification, is emerging as a key regulator of oxidative stress [39]. Interestingly, parallel to the OGD treatment of the DPSC and MSC, when we examined the NLRP3 expression in the presence of NLRP3-siRNA and SIRT3-siRNA, respectively, we observed that when DPSC and MSC were knocked down with NLRP3-siRNA, this led to a down regulation of the SIRT3 expression (Figures 4C and D), while when SIRT3 was knocked down, there was an inverse relationship between SIRT3 and NLRP3 expression (Figures 4E and F). Our immuno-cytoflourescence tests corroborated these findings. In summary, we discovered that knocking down SIRT3 reduces its expression in DPSC, whereas MCC950 marginally increases

it. Similarly, to the western blotting studies, immunofluorescence imaging revealed that SIRT3 regulates NLRP3 expression in an inverse way (Figure S3A and B). This led us to conclude that MCC950 regulates the inflammasome cascade through regulating SIRT3, which in turn regulates the expression of inflammasome proteins.

Discussion

The current study's experiments were carried out to investigate the effect of OGD on the fate of the stem cells *in vitro*. By investigating the effect of NLRP3 inflammation on human DPSC and MSC, we studied the effects of OGD on these cells. It is worth noting that inflammatory stress, such as that observed during ischemia-reperfusion injury or ischemic stroke, frequently results in the assembly or interaction of NLRP3 inflammasome complex proteins. In previous studies, we and others demonstrated this phenomenon [21, 40-43]. We also examined MCC950's reparative properties, which were found to effectively reverse the effects of OGD-induced inflammatory damage on the stem cell types listed above. In brief, our findings showed that (i) OGD upregulated the NLRP3 inflammasome in human DPSC and MSC, (ii) MCC950 inhibited NLRP3 inflammation by reversing the NLRP3 and SIRT3 levels in human, (iii) MCC950 changed the activation ratio of NLRP3/SIRT3 levels in DPSC and MSC, and iv) MCC950 inhibits the NLRP3 inflammasome-mediated inflammatory responses in these cells by up-regulating SIRT3 levels.

In ischemic stroke therapy, interventions such as stem cell transplantation are gaining favour. However, pre-clinical and clinical investigations have demonstrated that stroke therapy developments are limited and inadequate. This could be because acute inflammation or an immune response, oxidative stress, excitotoxicity, hypoxia, or anoikis all develop in the first few days after transplantation, and these are all common causes of stem cell mortality. Interestingly, in the last few years, many studies have looked into the role of the NLRP3 inflammasome-mediated inflammation in ischemic stroke-induced injury [44-46]. Along these lines, the impact of NLRP3 inflammasome activation on stem cell fate has not yet been looked into. In this study, we looked at how NLRP3 inflammation affects human stem cells when they are used in experiments to treat stroke. While observing the stem cell death pattern in OGD treated DPSC and MSC, we observed a high rate of pyroptosis mediated cell death. As evidenced through

western blotting and imaging of cleaved caspase1 as well as cell viability assays, MCC950 treatment significantly reduced the pyroptosis rate of DPSC and MSC cells. Within the last few years, the NLRP3 inflammasome-mediated pyroptosis has been identified as a potential cause of cellular death [47]. To corroborate our findings, we utilized LPS as an inflammatory inducer.

Oxidative stress and inflammation are thought to be important components of acute and chronic neurodegenerative disorders [48]. Treatment with ROS inhibitors has been demonstrated to reduce NLRP3 inflammasome activation caused by cadmium, silica, and asbestos [49, 50]. In the present case, total and mitochondrial ROS levels in DPSC and MSC were found to be higher. A key finding was that supplementing with MCC950 reversed the ROS-induced cell death in both cell types, indicating that there is cross-talk existing between these two processes that we did not investigate in this study. Mito-TEMPO served as a positive control for MCC950 treatment. It likewise reduced mitochondrial ROS levels, confirming MCC950's anti-oxidative activity. Our findings contribute to research of a similar nature, irrespective of disease, on the involvement of ROS and the NLRP3 inflammasome, providing a potentially feasible target for inflammatory disease prevention and treatment.

Finally, our findings suggest that the SIRT3 plays an important role in OGD-induced mitochondrial-ROS generation and NLRP3 inflammasome activation *in vitro*. In the current findings, we explored the effect of ischemic stress on SIRT3 and its repercussions on human DPSC and MSC. We were astonished to see that MCC950 increases SIRT3 expression while lowering NLRP3 expression, which turned out to be crucial findings of the current study. The siRNA studies in parallel confirmed these findings. As a result, we concluded that MCC950's other major target is SIRT3, besides the NLRP3 inflammasome, and that MCC950 therapy inhibits inflammation stress through depleting the levels of the NLRP3 inflammasome complex while activating SIRT3. In summary, SIRT3 was found to be a key signalling pathway mediating ischemic stroke-induced NLRP3 inflammasome activation *in vitro*.

MCC950's protective effect on the stem cell population employed in ischemic stroke could be attributed to a reduction in pro-inflammatory signalling cascades, resulting in reduced local inflammation, SIRT3 activation, and reduced pyroptosis. While this research implies that

MCC950 could be employed as a stem cell lifespan treatment, there are a few things to keep in mind. First and foremost, MCC950's sterility, dosage, and incubation time in culture for optimal uptake by stem cells must all be considered if MCC950 is to be administered to stem cells prior to transplantation so that stem cells become more able to survive, integrate, and differentiate in the ischemic brain. We demonstrated that MCC950 could restore human DPSC and MSC in culture. Altogether, the outcomes of the multiple tests performed for this study bolster the belief in MCC950's capacity for reparation.

Overall, we discovered that the NLRP3 inflammasome is activated while the levels of SIRT3 are depleted in stem cells used to treat ischemic stroke, resulting in a reduction in their number. MCC950 appears to protect stem cells from OGD-induced oxidative stress and inflammation via activating SIRT3 and inhibiting NLRP3 inflammasome. Our collective findings shed light on a new avenue of research regarding the fate of stem cells during stress. In conclusion, the results indicate that MCC950 and other such specific NLRP3 inflammasome inhibitors could be of high-value to rescue stem cells subjected to oxidative and inflammatory stress.

Acknowledgments

We appreciate the technical assistance provided by Mr. Mohammad Danish Siddiqui.

Funding

We appreciate the hypoxic chamber we were able to purchase with grant number YSS/2015/001731 from the Science Engineering Research Board, Department of Science and Technology, Government of India.

Ethics approval

Cell culture work was used in the current study, which was conducted on established hMSC (cat# CL001) and hDPSC (cat# CL008) (purchased from Himedia Pvt. Ltd., Mumbai), intended for basic research.

Consent to participate

Not Applicable

Consent for publication

All authors have read and approved the manuscript for publication.

Conflict of Interest

The authors indicated no financial relationships.

Author Contributions:

S.S.R.: experiment planning, conception, design, and drafting of manuscript, visualization and revision. R.P.: acquisition of data, results preparation, analysis and interpretation of data. N.K., A.J.S.: acquisition of data, results preparation. A.Q.K., R.K., R.H., & J.B.: visualization and revision, analysis and interpretation of data. A.A.B.R.: Provided the drug, MCC950, voluntarily. M.A.K.: resources.

Data Availability

On reasonable request, the corresponding author will provide the datasets that support the study's findings.

References

1. Katan, M., & Luft, A. (2018). Global Burden of Stroke. *Seminars in neurology*, *38*(2), 208–211. https://doi.org/10.1055/s-0038-1649503
2. Lapchak, P. A., & Zhang, J. H. (2017). The High Cost of Stroke and Stroke Cytoprotection Research. *Translational stroke research*, *8*(4), 307–317. https://doi.org/10.1007/s12975-016-0518-y
3. Palomino-Antolin, A., Narros-Fernández, P., Farré-Alins, V., Sevilla-Montero, J., Decouty-Pérez, C., Lopez-Rodriguez, A. B., Fernández, N., Monge, L., Casas, A. I., Calzada, M. J., & Egea, J. (2022). Time-dependent dual effect of NLRP3 inflammasome in brain

ischaemia. *British journal of pharmacology*, *179*(7), 1395–1410. https://doi.org/10.1111/bph.15732

4. Lin, H. B., Li, F. X., Zhang, J. Y., You, Z. J., Xu, S. Y., Liang, W. B., & Zhang, H. F. (2021). Cerebral-Cardiac Syndrome and Diabetes: Cardiac Damage After Ischemic Stroke in Diabetic State. *Frontiers in immunology*, *12*, 737170. https://doi.org/10.3389/fimmu.2021.737170
5. Kerr, N., Dietrich, D. W., Bramlett, H. M., & Raval, A. P. (2019). Sexually dimorphic microglia and ischemic stroke. *CNS neuroscience & therapeutics*, *25*(12), 1308–1317. https://doi.org/10.1111/cns.13267
6. Dugue, R., Nath, M., Dugue, A., & Barone, F. C. (2017). Roles of Pro- and Anti-inflammatory Cytokines in Traumatic Brain Injury and Acute Ischemic Stroke. In (Ed.), Mechanisms of Neuroinflammation. IntechOpen. https://doi.org/10.5772/intechopen.70099
7. Iadecola, C., & Anrather, J. (2011). The immunology of stroke: from mechanisms to translation. *Nature medicine*, *17*(7), 796–808. https://doi.org/10.1038/nm.2399
8. Jin, R., Yang, G., & Li, G. (2010). Inflammatory mechanisms in ischemic stroke: role of inflammatory cells. *Journal of leukocyte biology*, *87*(5), 779–789. https://doi.org/10.1189/jlb.1109766
9. Wang, Q., Tang, X. N., & Yenari, M. A. (2007). The inflammatory response in stroke. *Journal of neuroimmunology*, *184*(1-2), 53–68. https://doi.org/10.1016/j.jneuroim.2006.11.014
10. Hong, P., Gu, R. N., Li, F. X., Xiong, X. X., Liang, W. B., You, Z. J., & Zhang, H. F. (2019). NLRP3 inflammasome as a potential treatment in ischemic stroke concomitant with diabetes. *Journal of neuroinflammation*, *16*(1), 121. https://doi.org/10.1186/s12974-019-1498-0
11. Guekht, A., Skoog, I., Edmundson, S., Zakharov, V., & Korczyn, A. D. (2017). Artemida Trial (A Randomized Trial of Efficacy, 12 Months International Double-Blind Actovegin): A Randomized Controlled Trial to Assess the Efficacy of Actovegin in Poststroke Cognitive Impairment. *Stroke*, *48*(5), 1262–1270. https://doi.org/10.1161/STROKEAHA.116.014321
12. Zhang, X. L., Zhang, X. G., Huang, Y. R., Zheng, Y. Y., Ying, P. J., Zhang, X. J., Lu, X., Wang, Y. J., & Zheng, G. Q. (2021). Stem Cell-Based Therapy for Experimental Ischemic

Stroke: A Preclinical Systematic Review. *Frontiers in cellular neuroscience*, *15*, 628908. https://doi.org/10.3389/fncel.2021.628908

13. Kawabori, M., Shichinohe, H., Kuroda, S., & Houkin, K. (2020). Clinical Trials of Stem Cell Therapy for Cerebral Ischemic Stroke. *International journal of molecular sciences*, *21*(19), 7380. https://doi.org/10.3390/ijms21197380
14. Raza, S. S., Wagner, A. P., Hussain, Y. S., & Khan, M. A. (2018). Mechanisms underlying dental-derived stem cell-mediated neurorestoration in neurodegenerative disorders. *Stem cell research & therapy*, *9*(1), 245. https://doi.org/10.1186/s13287-018-1005-z
15. Surder, D., Manka, R., Moccetti, T., Lo Cicero, V., Emmert, M. Y., Klersy, C., Soncin, S., Turchetto, L., Radrizzani, M., Zuber, M., Windecker, S., Moschovitis, A., Bühler, I., Kozerke, S., Erne, P., Lüscher, T. F., & Corti, R. (2016). Effect of Bone Marrow-Derived Mononuclear Cell Treatment, Early or Late After Acute Myocardial Infarction: Twelve Months CMR and Long-Term Clinical Results. *Circulation research*, *119*(3), 481–490. https://doi.org/10.1161/CIRCRESAHA.116.308639
16. Mansour S. (2016). Autologous bone marrow mononuclear stem cells for acute myocardial infarction: is it only about time?. *European heart journal*, *37*(3), 264–266. https://doi.org/10.1093/eurheartj/ehv541
17. Dang, S., Xu, H., Xu, C., Cai, W., Li, Q., Cheng, Y., Jin, M., Wang, R. X., Peng, Y., Zhang, Y., Wu, C., He, X., Wan, B., & Zhang, Y. (2014). Autophagy regulates the therapeutic potential of mesenchymal stem cells in experimental autoimmune encephalomyelitis. *Autophagy*, *10*(7), 1301–1315. https://doi.org/10.4161/auto.28771
18. Lee, T. J., Shim, M. S., Yu, T., Choi, K., Kim, D. I., Lee, S. H., & Bhang, S. H. (2018). Bioreducible Polymer Micelles Based on Acid-Degradable Poly(ethylene glycol)-poly(amino ketal) Enhance the Stromal Cell-Derived Factor-1α Gene Transfection Efficacy and Therapeutic Angiogenesis of Human Adipose-Derived Stem Cells. *International journal of molecular sciences*, *19*(2), 529. https://doi.org/10.3390/ijms19020529
19. Prakash, R., Fauzia, E., Siddiqui, A. J., Yadav, S. K., Kumari, N., Singhai, A., Khan, M. A., Janowski, M., Bhutia, S. K., & Raza, S. S. (2021). Oxidative Stress Enhances Autophagy-Mediated Death Of Stem Cells Through Erk1/2 Signaling Pathway - Implications For Neurotransplantations. *Stem cell reviews and reports*, *17*(6), 2347–2358. https://doi.org/10.1007/s12015-021-10212-z

20. Paneni, F., Costantino, S., Kränkel, N., Cosentino, F., & Lüscher, T. F. (2016). Reprogramming ageing and longevity genes restores paracrine angiogenic properties of early outgrowth cells. *European heart journal*, *37*(22), 1733–1737. https://doi.org/10.1093/eurheartj/ehw073
21. Coll, R. C., Robertson, A. A., Chae, J. J., Higgins, S. C., Muñoz-Planillo, R., Inserra, M. C., Vetter, I., Dungan, L. S., Monks, B. G., Stutz, A., Croker, D. E., Butler, M. S., Haneklaus, M., Sutton, C. E., Núñez, G., Latz, E., Kastner, D. L., Mills, K. H., Masters, S. L., Schroder, K., … O'Neill, L. A. (2015). A small-molecule inhibitor of the NLRP3 inflammasome for the treatment of inflammatory diseases. Nature medicine, 21(3), 248–255. https://doi.org/10.1038/nm.3806
22. Guo, H., Callaway, J. B., & Ting, J. P. (2015). Inflammasomes: mechanism of action, role in disease, and therapeutics. Nature medicine, 21(7), 677–687. https://doi.org/10.1038/nm.3893
23. Tapia-Abellán, A., Angosto-Bazarra, D., Martínez-Banaclocha, H., de Torre-Minguela, C., Cerón-Carrasco, J. P., Pérez-Sánchez, H., Arostegui, J. I., & Pelegrin, P. (2019). MCC950 closes the active conformation of NLRP3 to an inactive state. Nature chemical biology, 15(6), 560–564. https://doi.org/10.1038/s41589-019-0278-6
24. Coll, R. C., Hill, J. R., Day, C. J., Zamoshnikova, A., Boucher, D., Massey, N. L., Chitty, J. L., Fraser, J. A., Jennings, M. P., Robertson, A. A. B., & Schroder, K. (2019). MCC950 directly targets the NLRP3 ATP-hydrolysis motif for inflammasome inhibition. Nature chemical biology, 15(6), 556–559. https://doi.org/10.1038/s41589-019-0277-7
25. Jiang, Q., Geng, X., Warren, J., Eugene Paul Cosky, E., Kaura, S., Stone, C., Li, F., & Ding, Y. (2020). Hypoxia Inducible Factor-1α (HIF-1α) Mediates NLRP3 Inflammasome-Dependent-Pyroptotic and Apoptotic Cell Death Following Ischemic Stroke. Neuroscience, 448, 126–139. https://doi.org/10.1016/j.neuroscience.2020.09.036
26. Radak, D., Katsiki, N., Resanovic, I., Jovanovic, A., Sudar-Milovanovic, E., Zafirovic, S., Mousad, S. A., & Isenovic, E. R. (2017). Apoptosis and Acute Brain Ischemia in Ischemic Stroke. Current vascular pharmacology, 15(2), 115–122. https://doi.org/10.2174/1570161115666161104095522
27. Wang, M., Liang, X., Cheng, M., Yang, L., Liu, H., Wang, X., Sai, N., & Zhang, X. (2019). Homocysteine enhances neural stem cell autophagy in in vivo and in vitro model of ischemic stroke. Cell death & disease, 10(8), 561. https://doi.org/10.1038/s41419-019-1798-4

28. Prakash, R., Mishra, R. K., Ahmad, A., Khan, M. A., Khan, R., & Raza, S. S. (2021). Sivelestat-loaded nanostructured lipid carriers modulate oxidative and inflammatory stress in human dental pulp and mesenchymal stem cells subjected to oxygen-glucose deprivation. Materials science & engineering. C, Materials for biological applications, 120, 111700. https://doi.org/10.1016/j.msec.2020.111700
29. Orellana-Urzúa, S., Rojas, I., Líbano, L., & Rodrigo, R. (2020). Pathophysiology of Ischemic Stroke: Role of Oxidative Stress. *Current pharmaceutical design*, *26*(34), 4246–4260. https://doi.org/10.2174/1381612826666200708133912
30. Zhao, W., Ma, L., Cai, C., & Gong, X. (2019). Caffeine Inhibits NLRP3 Inflammasome Activation by Suppressing MAPK/NF-κB and A2aR Signaling in LPS-Induced THP-1 Macrophages. *International journal of biological sciences*, *15*(8), 1571–1581. https://doi.org/10.7150/ijbs.34211
31. He, Y., Hara, H., & Núñez, G. (2016). Mechanism and Regulation of NLRP3 Inflammasome Activation. *Trends in biochemical sciences*, *41*(12), 1012–1021. https://doi.org/10.1016/j.tibs.2016.09.002
32. Li, F., Ma, Q., Zhao, H., Wang, R., Tao, Z., Fan, Z., Zhang, S., Li, G., & Luo, Y. (2018). L-3-n-Butylphthalide reduces ischemic stroke injury and increases M2 microglial polarization. *Metabolic brain disease*, *33*(6), 1995–2003. https://doi.org/10.1007/s11011-018-0307-2
33. Wang, Y. G., Fang, W. L., Wei, J., Wang, T., Wang, N., Ma, J. L., & Shi, M. (2013). The involvement of NLRX1 and NLRP3 in the development of nonalcoholic steatohepatitis in mice. *Journal of the Chinese Medical Association : JCMA*, *76*(12), 686–692. https://doi.org/10.1016/j.jcma.2013.08.010
34. Schumann, R. R., Belka, C., Reuter, D., Lamping, N., Kirschning, C. J., Weber, J. R., & Pfeil, D. (1998). Lipopolysaccharide activates caspase-1 (interleukin-1-converting enzyme) in cultured monocytic and endothelial cells. *Blood*, *91*(2), 577–584. https://doi.org/10.1182/blood.V91.2.577
35. Wang, F., Liang, Q., Ma, Y., Sun, M., Li, T., Lin, L., Sun, Z., & Duan, J. (2022). Silica nanoparticles induce pyroptosis and cardiac hypertrophy via ROS/NLRP3/Caspase-1 pathway. *Free radical biology & medicine*, *182*, 171–181. https://doi.org/10.1016/j.freeradbiomed.2022.02.027

36. Kinra, M., Nampoothiri, M., Arora, D., & Mudgal, J. (2022). Reviewing the importance of TLR-NLRP3-pyroptosis pathway and mechanism of experimental NLRP3 inflammasome inhibitors. *Scandinavian journal of immunology*, *95*(2), e13124. https://doi.org/10.1111/sji.13124
37. Wu, X., Gong, L., Xie, L., Gu, W., Wang, X., Liu, Z., & Li, S. (2021). NLRP3 Deficiency Protects Against Intermittent Hypoxia-Induced Neuroinflammation and Mitochondrial ROS by Promoting the PINK1-Parkin Pathway of Mitophagy in a Murine Model of Sleep Apnea. *Frontiers in immunology*, *12*, 628168. https://doi.org/10.3389/fimmu.2021.628168
38. Zhou, R., Yazdi, A. S., Menu, P., & Tschopp, J. (2011). A role for mitochondria in NLRP3 inflammasome activation. *Nature*, *469*(7329), 221–225. https://doi.org/10.1038/nature09663
39. Bause, A. S., & Haigis, M. C. (2013). SIRT3 regulation of mitochondrial oxidative stress. *Experimental gerontology*, *48*(7), 634–639. https://doi.org/10.1016/j.exger.2012.08.007
40. Skinner, O. P., Jurczyluk, J., Baker, P. J., Masters, S. L., Rios Wilks, A. G., Clearwater, M. S., Robertson, A. A. B., Schroder, K., Mehr, S., Munoz, M. A., & Rogers, M. J. (2019). Lack of protein prenylation promotes NLRP3 inflammasome assembly in human monocytes. *The Journal of allergy and clinical immunology*, *143*(6), 2315–2317.e3. https://doi.org/10.1016/j.jaci.2019.02.013
41. Arbore, G., West, E. E., Spolski, R., Robertson, A. A. B., Klos, A., Rheinheimer, C., Dutow, P., Woodruff, T. M., Yu, Z. X., O'Neill, L. A., Coll, R. C., Sher, A., Leonard, W. J., Köhl, J., Monk, P., Cooper, M. A., Arno, M., Afzali, B., Lachmann, H. J., Cope, A. P., … Kemper, C. (2016). T helper 1 immunity requires complement-driven NLRP3 inflammasome activity in $CD4^+$ T cells. *Science (New York, N.Y.)*, *352*(6292), aad1210. https://doi.org/10.1126/science.aad1210
42. Fauzia E, Barbhuyan TK, Shrivastava AK, Kumar M, Garg P, Khan MA, Robertson AAB, Raza SS. Chick Embryo: A Preclinical Model for Understanding Ischemia-Reperfusion Mechanism. Front Pharmacol. 2018 Sep 21;9:1034.
43. van Hout, G. P., Bosch, L., Ellenbroek, G. H., de Haan, J. J., van Solinge, W. W., Cooper, M. A., Arslan, F., de Jager, S. C., Robertson, A. A., Pasterkamp, G., & Hoefer, I. E. (2017). The selective NLRP3-inflammasome inhibitor MCC950 reduces infarct size and preserves

cardiac function in a pig model of myocardial infarction. *European heart journal*, *38*(11), 828–836. https://doi.org/10.1093/eurheartj/ehw247

44. Che Mohd Nassir, C. M. N., Zolkefley, M. K. I., Ramli, M. D., Norman, H. H., Abdul Hamid, H., & Mustapha, M. (2022). Neuroinflammation and COVID-19 Ischemic Stroke Recovery-Evolving Evidence for the Mediating Roles of the ACE2/Angiotensin-(1-7)/Mas Receptor Axis and NLRP3 Inflammasome. *International journal of molecular sciences*, *23*(6), 3085. https://doi.org/10.3390/ijms23063085
45. Chen, X., Wang, Y., Yao, N., & Lin, Z. (2022). Immunoproteasome modulates NLRP3 inflammasome-mediated neuroinflammation under cerebral ischaemia and reperfusion conditions. *Journal of cellular and molecular medicine*, *26*(2), 462–474. https://doi.org/10.1111/jcmm.17104
46. Li, F., Xu, D., Hou, K., Gou, X., Lv, N., Fang, W., & Li, Y. (2021). Pretreatment of Indobufen and Aspirin and their Combinations with Clopidogrel or Ticagrelor Alleviates Inflammasome Mediated Pyroptosis Via Inhibiting NF-κB/NLRP3 Pathway in Ischemic Stroke. *Journal of neuroimmune pharmacology : the official journal of the Society on NeuroImmune Pharmacology*, *16*(4), 835–853. https://doi.org/10.1007/s11481-020-09978-9
47. Wang, Y., Gao, W., Shi, X., Ding, J., Liu, W., He, H., Wang, K., & Shao, F. (2017). Chemotherapy drugs induce pyroptosis through caspase-3 cleavage of a gasdermin. *Nature*, *547*(7661), 99–103. https://doi.org/10.1038/nature22393
48. Solleiro-Villavicencio, H., & Rivas-Arancibia, S. (2018). Effect of Chronic Oxidative Stress on Neuroinflammatory Response Mediated by $CD4^{+}$T Cells in Neurodegenerative Diseases. *Frontiers in cellular neuroscience*, *12*, 114. https://doi.org/10.3389/fncel.2018.00114
49. Chen, H., Lu, Y., Cao, Z., Ma, Q., Pi, H., Fang, Y., Yu, Z., Hu, H., & Zhou, Z. (2016). Cadmium induces NLRP3 inflammasome-dependent pyroptosis in vascular endothelial cells. *Toxicology letters*, *246*, 7–16. https://doi.org/10.1016/j.toxlet.2016.01.014
50. Dostert, C., Pétrilli, V., Van Bruggen, R., Steele, C., Mossman, B. T., & Tschopp, J. (2008). Innate immune activation through Nalp3 inflammasome sensing of asbestos and silica. *Science (New York, N.Y.)*, *320*(5876), 674–677. https://doi.org/10.1126/science.1156995

Legends

Figure 1. MCC950 mitigated OGD induced $O_2^{\bullet-}$, H_2O_2 and total ROS generation while restoring the DPSC and MSC morphology. Immunofluorescence microscopy and spectrophotometry were used to investigate OGD-induced $O_2^{\bullet-}$, H_2O_2 and total ROS production in DPSC and MSC. Figure A & D shows the levels of $O_2^{\bullet-}$ in the presence and absence of MCC950 and LPS in DPSC and MSC (Figure A and D, 9 replicates = 3 biological + 6 technical, at least 50 cells/group). Figure B represents H_2O_2 levels in DPSC (8 biological replicates), while Figure C & F represents the levels of total ROS in the presence and absence of MCC950 and LPS in DPSC and MSC (Figure C and F, 9 replicates = 4 biological + 5 technical, at least 50 cells/group). Figure E represents H_2O_2 level in MSC (8 biological replicates). In brief, the above results demonstrate that $O_2^{\bullet-}$, H_2O_2, and total ROS, generation are increased in both cell types treated to OGD when compared to controls. However, the addition of MCC950 considerably reversed the impact. LPS treatment had the same impact as OGD treatment. Figure G and H represent the morphological changes observed in DPSC and MSC in the presence and absence of MCC950. LPS again served as a positive control. The pictures were taken at 20X magnification—scale bars=50μm. The error bars represent the mean±SD.

Figure 2. MCC950 attenuated OGD induced NLRP3 inflammation in DPSC and MSC. Activation of the NLRP3 inflammasome (NLRP3, ASC, cleaved caspase1, IL-1β, and IL-18) was successfully attenuated by the supplementation of MCC950 in DPSC and MSC, as analyzed by western blot (Figure A (n=9, replicates, 4 biological + 5 technical for NLRP3, ASC, IL-1β, IL-18, and n=5, 4 biological + 1 technical for cleaved caspase1), and Figure B (n=8, 4 biological + 4 technical for NLRP3, ASC, IL-1β, IL-18, and n=6, 4 biological + 2 technical for cleaved

caspase1). Figure C (n=9, replicates, 4 biological + 5 technical, at least 50 cells/group) represents the activation of NLRP3 post-OGD treatment in DPSC, while Figure E (n=9, replicates, 4 biological + 5 technical, at least 50 cells/group) represents the expression of NLRP3 in MSC treated OGD cells. The addition of MCC950 significantly down-regulated the NLRP3-expression in both cell types. Likewise, when cleaved caspase1 was examined under OGD treatment, the mean intensity fluorescence (MIF) was found to be high in the OGD treated DPSC (Figure D; n=9, 4 biological + 5 technical, at least 50 cells/group) as well as MSC (Figure F; n=9, 4 biological + 5 technical, at least 50 cells/group). The supplementation of MCC950 effectively impeded the activation of caspase1. The LPS yielded a similar outcome as the OGD. The pictures were taken at 40X magnification—scale bars=20μm. The error bars represent mean±SD.

Figure 3. MCC950 enhances DPSC and MSC survival. The cell viability assay was performed in DPSC and MSC using Trypan blue exclusion dye, the MTT assay, and BrdU Tunel assays. Figure A and C represent the MTT assay for DPSC (n=8, 4 biological + 4 technical) and MSC (n=8, 4 biological + 4 technical). For MTT estimation, groups receiving OGD showed significantly reduced cell numbers (compared to their control). At the same time, the supplementation of MCC950 significantly enhanced the survival rate in OGD treated cells as compared to the control. The difference, however, was significantly lower when comparing it with the OGD alone DPSC or MSC cells. Figure B represents the Tunel staining in DPSCs. The results were in line with the MTT results. In brief, the Tunel positive cells were high in number in the OGD treated group, while MCC950 significantly reduced them (n=4 biological replicates, at least 50 cells/group). Figure D represents a high MSC number in the OGD+MCC950 treated MSCs compared to the OGD alone treated MSCs (n=8, 4 biological + 4 technical) as measured

by trypan blue staining. The pictures for figure B were taken at 40X magnification —scale bars=20µm, while for figure D at 10X magnification—scale bars=100µm. The error bars represent the mean±SD.

Figure 4. MCC950 impedes mitochondrial ROS and NLRP3 expression while maintaining the mitochondrial mass and SIRT3 levels in DPSC and MSC. Following the appropriate treatments, the mitochondrial ROS and mitochondrial mass were measured by labeling the cells with mito-SOX. The mitoTracker Green was used to identify the mitochondria as well as the mitochondrial mass. The results showed a significant decrease in the mitochondrial ROS generation with the supplementation of MCC950 in DPSC (n=9, 4 biological + 5 technical, at least 50 cells/group; Figure A), and MSC (n=9, 4 biological + 5 technical, at least 50 cells/group; Figure B). mito-TEMPO was used as a negative control, and yielded similar results as the MCC950 treated cells. Interestingly, MCC950 was able to maintain the mitochondrial mass compared to the OGD-treated cells. Western blots data revealed that MCC950 significantly impeded the expression of the NLRP3, while enhancing the SIRT3 level in both DPSC (Figure C) and MSC (Figure D). Interestingly, the results further indicated that downregulating SIRT3 upregulated NLRP3 (Figures E and F). n=5, 4 biological + 1 technical for C, D and n=6, 4 biological + 2 technical for E, F for NLRP3 and for SIRT3. The pictures were taken at 20X magnification—scale bars = 50µm. The error bars represent the mean±SD.

Fig 5: Graphical Abstract. The oxidative and inflammatory events associated with OGD are depicted in this diagram. The 12 hours of OGD followed by 24 hours of the normoxia treatment lead to NLRP3 mediated inflammation. While the supplementation of MCC950 efficiently

reduced the inflammation through inhibiting the expression of the NLRP3 inflammasome while enhancing the SIRT3 expression level, thereby reducing the cell death number *in vitro*.

Figure S1. Generation of OGD-induced $O_2^{\bullet-}$ and H_2O_2 and total ROS was due to the NLRP3 inflammation. To confirm that OGD induced $O_2^{\bullet-}$ and H_2O_2 and total ROS generation was linked to the NLRP3 inflammasome activation, we examined the ratio of the abovementioned ROS in the presence and absence of NLRP3-siRNA. The use of NLRP3-siRNA confirmed the involvement of the NLRP3 inflammation pathway in ROS production, as determined by DHE, Amplex Red, and DCFDA (Figures A-C; 9 replicates = 4 biological + 5 technical, at least 50 cells/group for figure A and B, for Figure C n=8; replicates = 4 biological + 4 technical).The figure D represents morphology of DPSC. The pictures were taken at 20X magnification—scale bars=50µm. The error bars represent the mean±SD.

Figure S2. Confirmation of the participation of the NLRP3 inflammasome in the impaired DPSC and MSC. Transfection with NLRP3-siRNA inhibited OGD induced expression of NLRP3, ASC, and cleaved caspase1 expression (the three most important proteins of the NLRP3 inflammasome pathway), thereby, confirming the participation of the NLRP3 inflammasome. In DPSC (Figure A) and MSC (Figure B).

Figure S3. MCC950 regulates NLRP3 expression in human DPSC through modulating SIRT3 expression. In the presence and absence of SIRT3-siRNAs, we examined the effects of MCC950 infusion on NLRP3 and SIRT3 down-regulated DPSC. We observed that MCC950 was able to reverse the expression of the SIRT3 (Figure A) and NLRP3 (Figure B) in siSIRT3-knock down-DPSC as compared to the OGD alone treated DPSC. 9 replicates = 4 biological + 5

technical. The pictures were taken at 40X magnification—scale bars=20µm. The error bars represent the mean±SD.

Figure S4. Evaluation of NLRP3 expression at various time points. We investigated the effects NLRP3 expression in the presence and absence of MCC950 at various time points during OGD. NLRP3 expression increased from 0 to 12 hours of OGD under control conditions, but was significantly reduced by MCC950. The error bars represent the mean±SD, n=3.

Figure 1

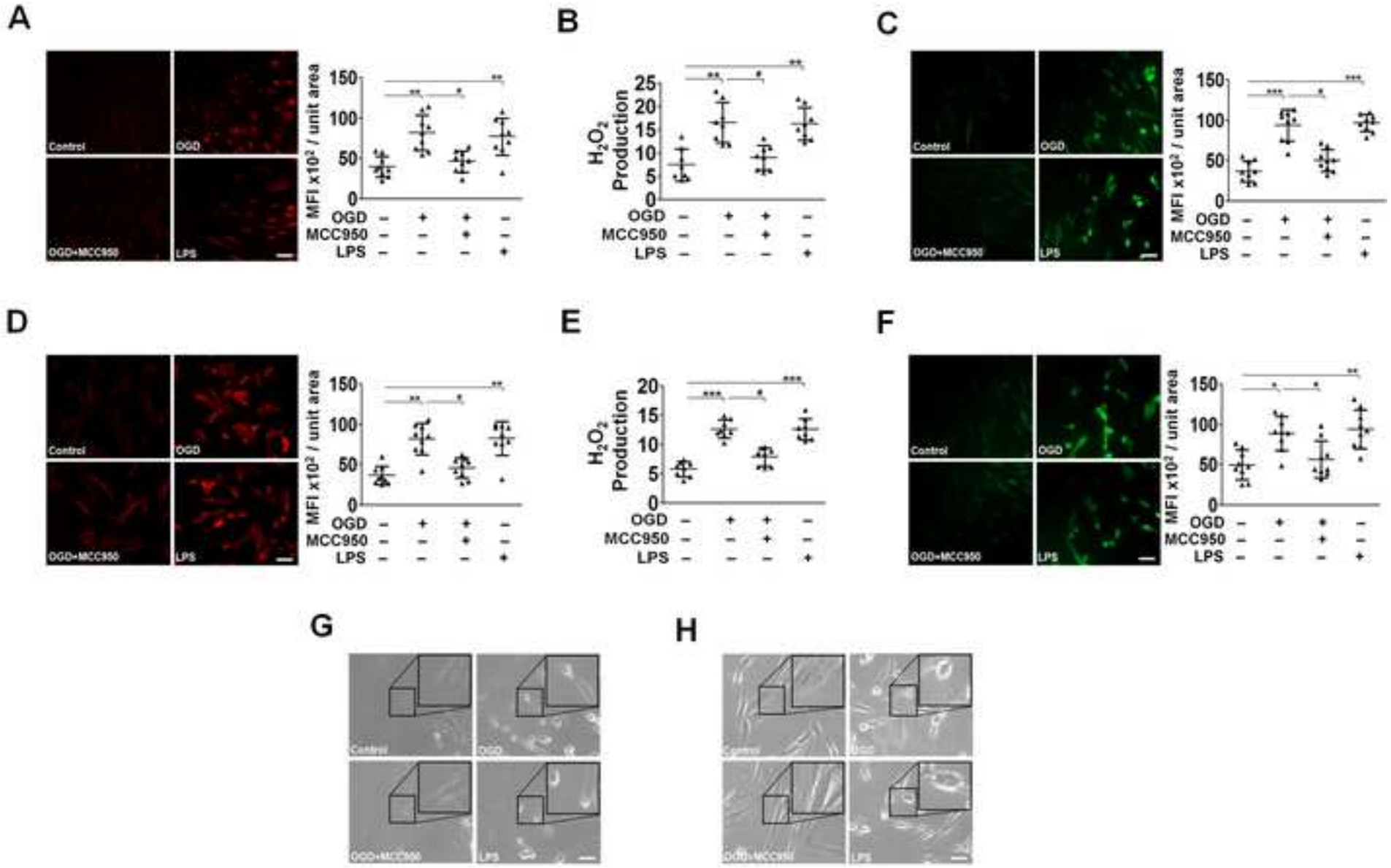

Figure 2

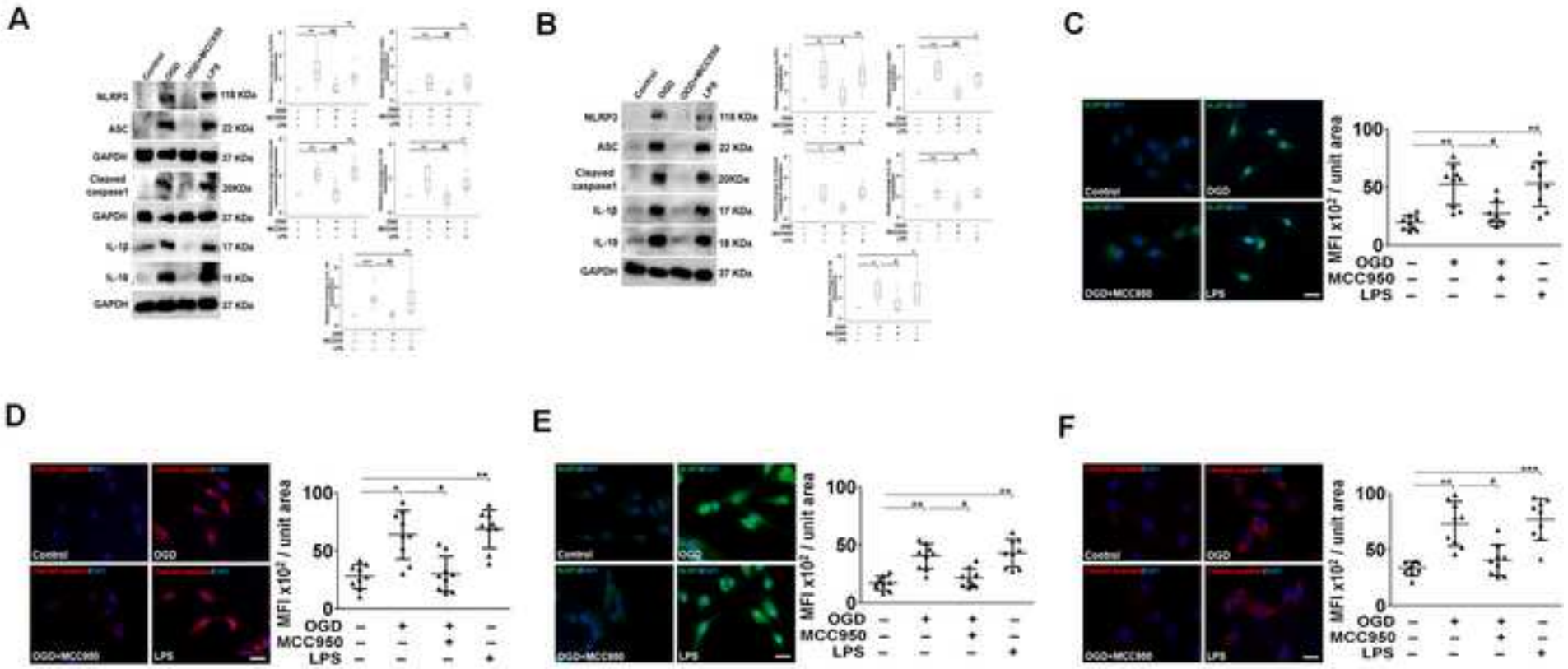

Figure 3

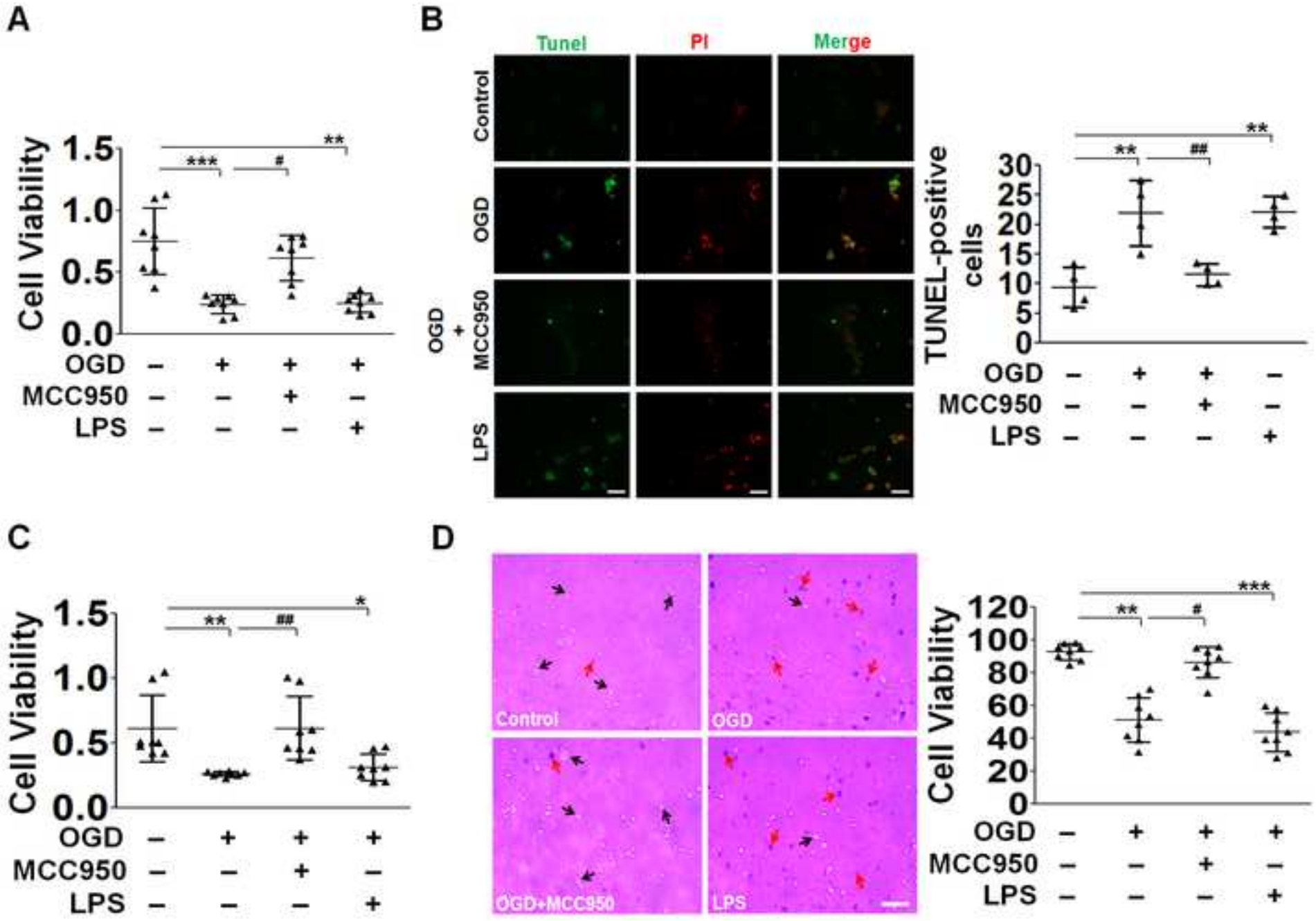

Figure 4

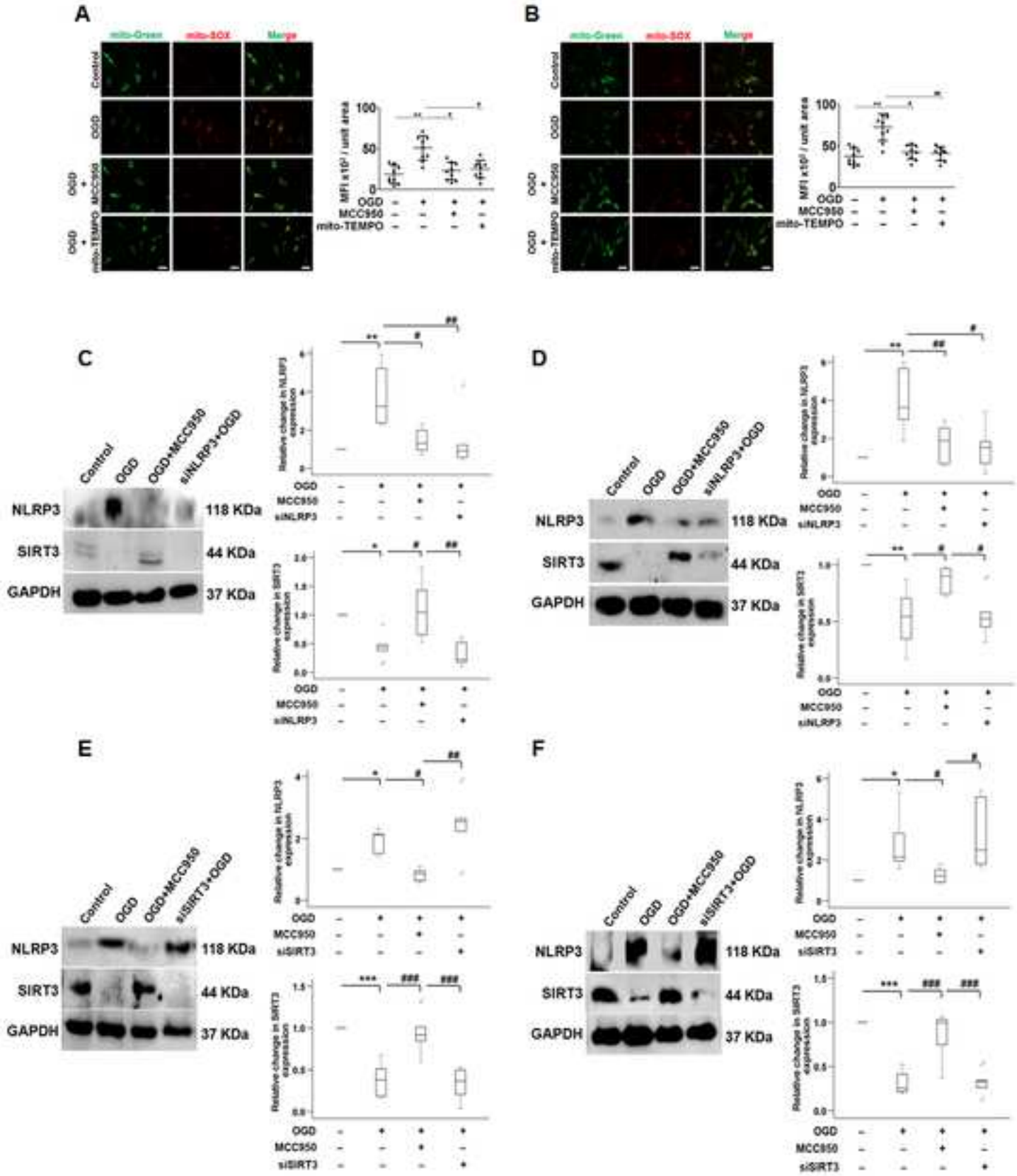

Supplementary Figure S1

Click here to access/download

Supplementary Material

Fig_S1.tif

Supplementary Figure S2

Supplementary Figure S3

Supplementary Figure S4

Supplementary Table ST2

Graphical Abstract